Journal of Alloys and Compounds 509 (2011) 7247–7252

Contents lists available at ScienceDirect

Journal of Alloys and Compounds

journal homepage: www.elsevier.com/locate/jallcom

Effect of $LiSbO_3$ on the phase structure, microstructure and electric properties of $Sr_{0.53}Ba_{0.47}Nb_2O_6$ ceramics

Lingling Wei, Zupei Yang*, Rui Gu, Xuejuan Yan, Yongqiang Li

Key Laboratory for Macromolecular Science of Shaanxi Province, School of Chemistry and Materials Science, Shaanxi Normal University, Xi'an 710062, Shaanxi, PR China

ARTICLE INFO

Article history:
Received 27 September 2010
Received in revised form 24 March 2011
Accepted 28 March 2011
Available online 5 April 2011

Keywords:
Ceramics
Tungsten bronze structure
Dielectric properties
Ferroelectric properties
X-ray diffraction

ABSTRACT

$LiSbO_3$ doped $Sr_{0.53}Ba_{0.47}Nb_2O_6$ ceramics were synthesized by conventional mixed-oxide method. The phase structure, microstructure, dielectric and ferroelectric properties of obtained ceramics were investigated. Pure tungsten bronze structure could be obtained in all ceramics and $LiSbO_3$ additive could promote densification and reduce the sintering temperature. The dielectric characteristics showed diffuse phase transition phenomena for all samples, which was proved by linear fitting of the modified Curie–Weiss law with γ value varying between 1.65 and 1.92. With increasing $LiSbO_3$ content, the transition temperature T_c decreased gradually to near room temperature. Normal ferroelectric hysteresis loops could be observed in all compositions, but the remnant polarization (P_r) and coercive field (E_c) all decreased gradually. Besides, the underlying mechanism for variations of the electrical properties caused by $LiSbO_3$ doping was explained in this work.

1. Introduction

Strontium barium niobate $Sr_xBa_{1-x}Nb_2O_6$ (SBN) is a ferroelectric solid solution between $BaNb_2O_6$ (BN) and $SrNb_2O_6$ (SN) which has a tungsten bronze (TB) structure with a unit-cell formula of $[(A1)_2(A2)_4C_4][(B1)_2(B2)_8]_{30}$. In the formula, A1, A2, B and C sites are 15-, 12-, 6- and 9-fold coordinated oxygen octahedral sites in the crystal lattice structure, respectively, where the A1 and A2 sites can be occupied by Sr^{2+}, Ba^{2+}, Ca^{2+}, Pb^{2+}, K^+, Na^+ and some rare earth cations, the B sites by either Nb^{5+} or Ta^{5+}, the C sites by Li^+ and other small cations. The smallest C sites are usually empty, then the formula $A_6B_{10}O_{30}$ is for the filled tungsten bronze structure [1]. For the structure of SBN, where only five A-sites are occupied out of six which result in a so-called unfilled structure that is responsible for charge disorder and relaxor behavior. It is reported that SBN can be obtained in a wide range of compositions ($0.25 \le x \le 0.75$). This allows us to adjust the Sr/Ba ratio to suit the different needs with appropriate physical and dielectric properties [2–4]. SBN is important in many technological applications such as electro-optic, pyroelectric, piezoelectric and photorefractive device because of its excellent pyroelectric and linear electro-optic coefficients [5–8]. Then, SBN has received considerable attention as a lead-free electroceramics.

The physical and electrical properties may vary significantly when doping or substituting desired impurities in SBN compounds [9–11]. For instance, Hao et al. [12] used low-temperature combustion synthesis process to prepare $Sr_{0.5}Ba_{0.5}Nb_2O_6$ ceramics and found that doping Na^+ and K^+ could increase the dielectric and ferroelectric properties. Jigajeni et al. [13] consisted of $Sr_{0.5}Ba_{0.5}Nb_2O_6$ and $Co_{0.7}Mg_{0.3}Fe_{1.8}Mn_{0.2}O_4$ to form new magnetoelectric composites. Yang et al. [14] reported that substitution of tantalum for niobium in B sites increased the sintering temperature to higher than 1400 °C, and also led to a great decrease in both the transition temperature and dielectric constant. As is well known, the tungsten bronze niobates ceramics are known to be very difficult in obtaining high density and good electrical properties by solid state reaction method due to the abnormal grain growth along with crack generation in sintering process, such as $Sr_{1-x}Ba_xNb_5O_{15}$ [15], $Sr_2KNb_5O_{15}$ [16,17], and $Pb_{1-x}Ba_xNb_5O_{15}$ [18] systems. The sintering temperature for SBN ceramics is higher than 1350 °C, which is benefit for abnormal grain growth and the crack generation caused by the appearance of molten area. This phenomenon has also been found in other tungsten bronze $Sr_2NaNb_5O_{15}$ niobates ceramics in our previous work [17,19]. In both lead-based and lead-free ceramic systems, $LiSbO_3$ is usually used as sintering additive to reduce the sintering temperature and improve the properties [20–22].

In addition, in our previous work, higher relative density and better properties were obtained in $Sr_xBa_{1-x}Nb_2O_6$ ceramics with $x = 0.53$ [12]. Until now, few reports on sintering temperature, dielectric and ferroelectric properties of SBN ceramics doping with $LiSbO_3$ are available. Then in this work, the study on structure, sintering temperature and properties of $Sr_{0.53}Ba_{0.47}Nb_2O_6$ ceramics (SBN53) doped with $LiSbO_3$ was presented. The effect of $LiSbO_3$ doping on phase formation, microstructure, sintering tempera-

* Corresponding author. Tel.: +86 29 8531 0352; fax: +86 29 8530 7774.
E-mail address: yangzp@snnu.edu.cn (Z. Yang).

0925-8388/$ – see front matter © 2011 Elsevier B.V. All rights reserved.
doi:10.1016/j.jallcom.2011.03.149

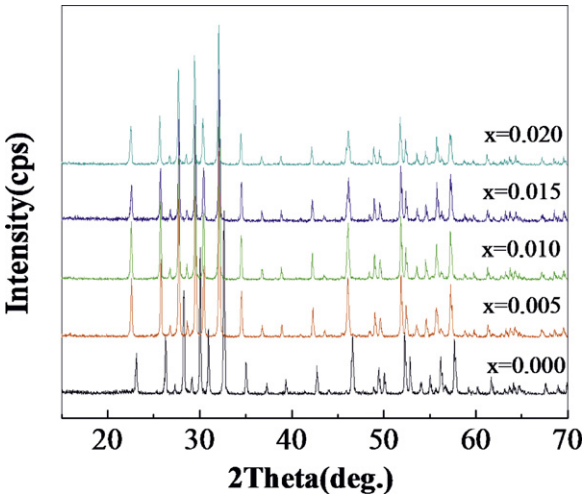

Fig. 1. XRD patterns of $(1-x/2)$ SBN53–xLS ceramics as a function of x.

ture, dielectric and ferroelectric properties of SBN53 ceramics were experimentally studied in detail.

2. Experimental

Conventional mixed-oxide method was used to prepare $(1-x/2)$ $Sr_{0.53}Ba_{0.47}Nb_2O_6$–$x$$LiSbO_3$ (x = 0.000, 0.005, 0.010, 0.015, and 0.020) (abbreviated as SBN53–LS) ceramics with reagent-grade powders of $SrCO_3$ (99%), $BaCO_3$ (99%), Nb_2O_5 (99.5%), Li_2CO_3 (98%) and Sb_2O_3 (99%). They were mixed by ball-milling in ethanol for 12 h using zirconia balls. The mixed powders were dried at 80 °C and calcined at 1180 °C for 4 h in air, respectively. Then, the synthesized SBN–LS particles were mixed with 5 wt% polyvinyl alcohol (PVA) solution and then pressed into pellets with a diameter of 15 mm under 300 MPa pressure. After burning out PVA at 500 °C, the green samples were sintered at 1250–1350 °C for 6 h in air, respectively.

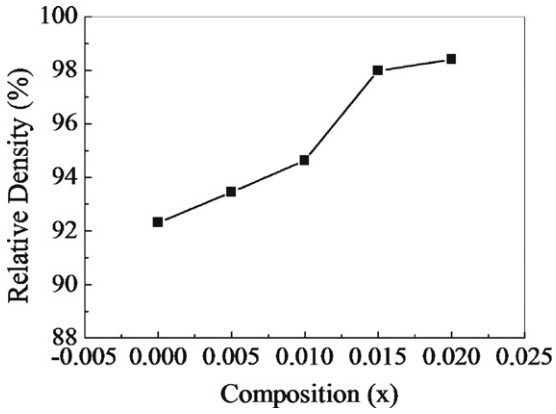

Fig. 2. Density of $(1-x/2)$ SBN53–xLS ceramics with different x sintered at 1300 °C.

The phase structure of ceramics was measured by X-ray diffraction (XRD, D/max-2200, Rigaku, Tokyo, Japan) with Cu $k\alpha$ radiation (step: 0.02°). The microstructure of the sintered ceramics was observed by scanning electron microscopy (SEM, Model Quanta 200, FEI Company, Eindhoven, the Netherlands).

Silver electrodes were formed on both surfaces of each sintered disk by firing at 850 °C for 30 min. Dielectric properties of the ceramics were obtained using an LCR meter ((Agilent 4284A)) by measuring capacitance C and dielectric loss $\tan\delta$ from room temperature to 300 °C at 1, 10 and 100 kHz, respectively. The polarization versus electric (P–E) hysteresis loops were observed by a Radiant Precision Workstation (USA).

3. Result and discussion

Fig. 1 shows the XRD patterns of the ceramics with different $LiSbO_3$ contents. As shown in Fig. 1, all ceramics are of single tungsten bronze (TB) structure and no second phase can be detected, which indicates that Li^+ and Sb^{5+} have diffused into the tungsten bronze structure lattice to form a solid solution. The diffraction

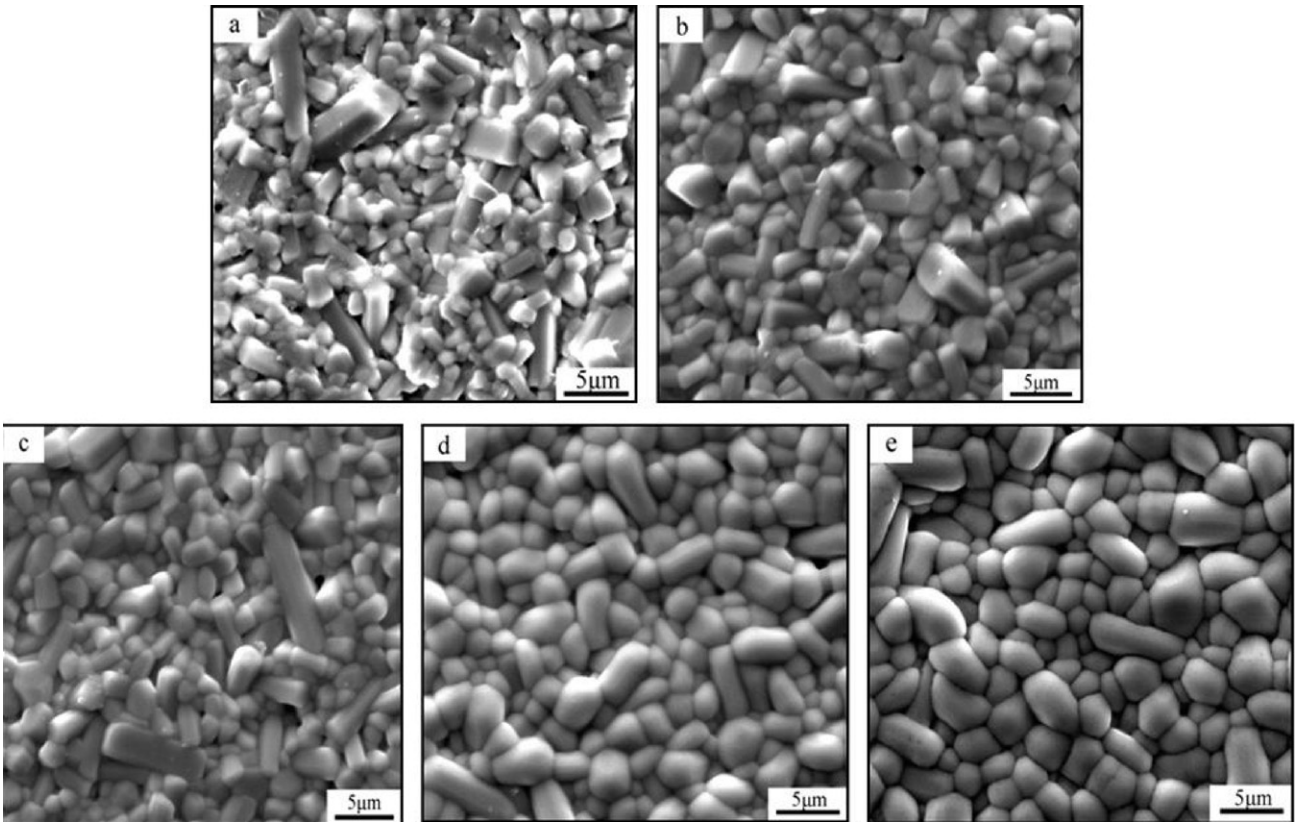

Fig. 3. SEM micrographs of $(1-x/2)$ SBN53–xLS ceramics sintered at 1300 °C: (a) x = 0.000, (b) x = 0.050, (c) x = 0.010, (d) x = 0.015, and (e) x = 0.020.

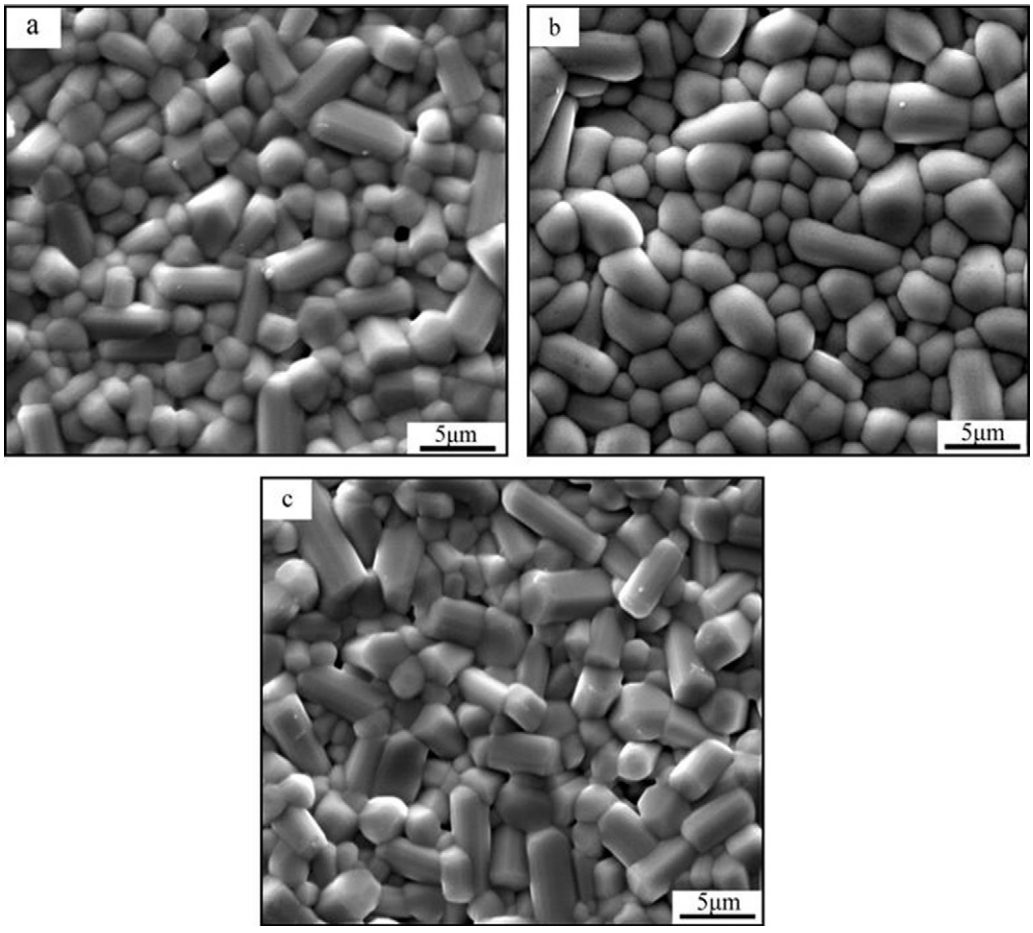

Fig. 4. SEM micrographs of $(1-x/2)$ SBN53–xLS ceramics with $x = 0.020$ sintered at different temperatures: (a) 1280 °C, (b) 1300 °C, and (c) 1330 °C.

peaks are indexed according to JCPDS # 73-0126. In tetragonal SBN crystal, Sr^{2+} ions (radius 1.12 Å) and Ba^{2+} ions (radius 1.35 Å) occupy the A sites, Nb^{5+} ions (radius 0.64 Å) occupy the B sites and form NbO_6 groups associated with six oxygen atoms. Taking the radius of doing Li^+ (radius 0.76 Å) into account, it is much smaller than that of A sites. Then it is reasonable that Li^+ ions occupy C sites and Sb^{5+} ions (radius 0.60 Å) substitute for Nb^{5+} ions and form the SbO_6 groups. In addition, the lattice parameters of the SBN ceramics with different $LiSbO_3$ contents were calculated using external Si standard method and Prague formula. The lattice parameters of SBN53–LS ceramics with $x = 0.005$ are $a = 12.462$ Å and $c = 3.937$ Å, while the lattice parameters of SBN53–LS ceramics with $x = 0.02$ are $a = 12.422$ Å and $c = 3.886$ Å, showing that the smaller radius of Li^+ and Sb^{5+} doping makes the unit cell size smaller and also makes distortion of the unit cells in SBN ceramics.

Fig. 2 shows the relative density of the SBN53–LS ceramics with different x ($x = 0.000$, 0.005, 0.010, 0.015, and 0.020) when sintered at the same sintering temperature of 1300 °C. The relative density was calculated based on the theoretical density of SBN52 (5.33 g/cm^3) [18]. It can be seen from Fig. 2 that for the SBN53–LS ceramics with $x = 0.000$, 0,005 and 0.010, the relative density is lower than 95%, indicating that the ceramics are not dense and the sintering temperature is low. With increasing x, the relative density increases gradually and reaches the maximum value of about 98.4% at $x = 0.020$. These results show that $LiSbO_3$ can promote densification and reduce the sintering temperature.

Fig. 3 shows the SEM micrographs of the SBN53–LS ceramics with different x ($x = 0.000$, 0.005, 0.010, 0.015, and 0.020) when sintered at the same sintering temperature of 1300 °C. It was found that by adding $LiSbO_3$ to $Sr_{0.53}Ba_{0.47}Nb_2O_6$, the grain size increases and the porosity decreases with increasing $LiSbO_3$ content. The variation of porosity in Fig. 3 is consistent with the density results in Fig. 2. According to Fig. 3(a)–(c), the high porosity and inhomogeneous grain size indicates that the sintering temperature of 1300 °C is lower for the ceramics with $x = 0.000$, 0.005 and 0.010. With further increasing x to 0.015 and 0.020, a characteristic tetragonal morphology of low porosity and uniform size can be obtained in Fig. 3(d) and (e) when the sintering temperature is 1300 °C, further showing that the $LiSbO_3$ doping can reduce the sintering temperature. Fig. 4 shows the microstructures of sample with $x = 0.020$ as a function of sintering temperature. As shown in Fig. 4, with increasing the sintering temperature, the pores become less and the grain grows bigger. The grains with regular grain size and less porosity can be obtained when the ceramics are sintered at 1300 °C. In addition, no abnormal grain growth along with crack generation can be found in Figs. 3 and 4.

Fig. 5 shows the temperature dependence of the dielectric constant ε_r in a range of frequencies for samples with different x ($x = 0.000$, 0.005, 0.010, 0.015, and 0.020). The dielectric characteristics show diffuse phase transition (DPT) phenomena (exhibit a broad Curie peak in the phase transition range). The positions of the maximum in the dielectric constant shift toward higher temperatures as the frequency increases. $Sr_xBa_{1-x}Nb_2O_6$ ceramics are well-known DPT relaxor materials [23]. The relaxor behavior in SBN53–LS ceramics should be attributed to the cationic disorder induced by substitutions. In the solid solution of SBN53–LS, Sr^{2+} and Ba^{2+} ions occupy the A sites, Li^+ ions occupy the C sites, Nb^{5+} and Sb^{5+} ions occupy the B sites of $[(A1)_2(A2)_4C_4][(B1)_2(B2)_8]_{30}$ in

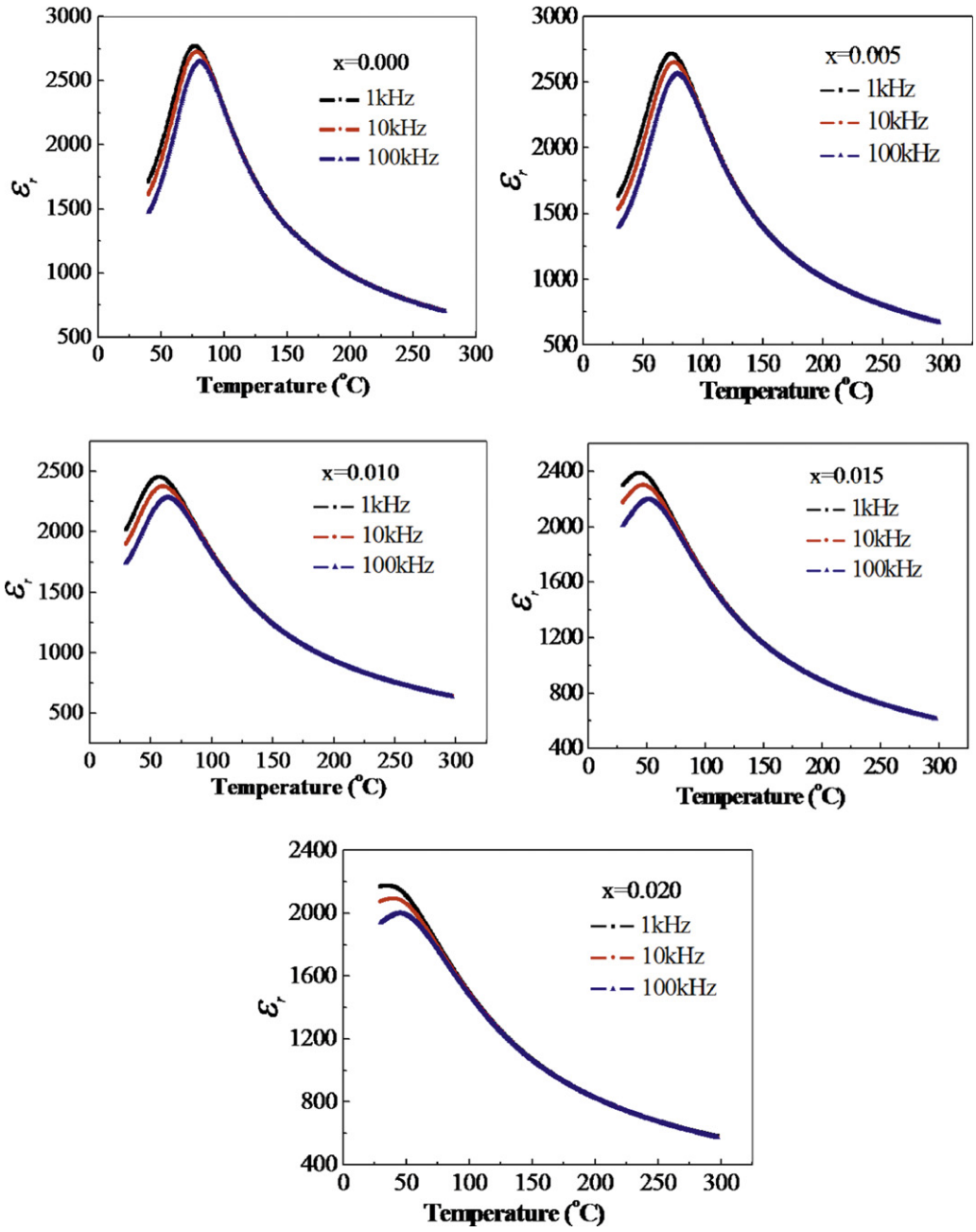

Fig. 5. Temperature dependence of dielectric constant for $(1-x/2)$ SBN53–xLS ceramics (x = 0.000, 0.005, 0.010, 0.015 and 0.020).

tungsten bronze structure. Therefore the ion disorder in the unit cell should be one of the reasons for the appearance of the frequency dispersion.

In order to further confirm the relaxor behavior of SBN53–LS ceramics, quantitative characterizations as described in the following have been done. The diffuseness of the phase transition can also be explained by the modified Curie–Weiss law: $1/\varepsilon - 1/\varepsilon_m = (T - T_m)^\gamma/C$, where ε_m is the peak value of dielectric constant and T_m is the phase transition temperature at which ε_r reaches the maximum. γ and C are assumed to be constant. γ is the degree of diffuseness, and C is the Curie-like constant. The degree of diffuseness γ can have a value ranging from 1 for a normal ferroelectric to 2 for an ideal relaxor ferroelectric. When $\gamma = 1$, the materials with this type phase transition belong to normal ferroelectrics; when $1 < \gamma < 2$, the materials belong to relaxor ferroelectrics; when $\gamma = 2$, the materials belong to ideal relaxor ferroelectric. The plots of $\ln[(\varepsilon_m/\varepsilon) - 1]$ versus $\ln(T - T_m)$ for the SBN53–LS ceramics (x = 0.000, 0.005, 0.010, 0.015, and 0.020) at 1 kHz are shown in Fig. 6. A linear relationship is observed in all samples. The slope of the fitting curves is used to determine the γ value. It can be seen that γ varies between 1.65 and 1.95 in all compositions, which indicates that all ceramics show intermediate relaxor-like behavior between normal and ideal relaxor ferroelectrics. It is in accordance with the results of Fig. 5.

Fig. 7 shows the variations of dielectric constant ε_r as a function of temperature (0–300 °C) at 1 kHz frequency for all SBN53–LS compositions. The dielectric constant increases with increasing temperature up to transition temperature (T_c) and then decreases with increasing temperature, which is normal behavior of ferroelectrics. The peaks of ε_r are associated to the ferroelectric tetragonal phase to paraelectric phase transition. Moreover, diffuse phase transition behavior is observed in every composition. The

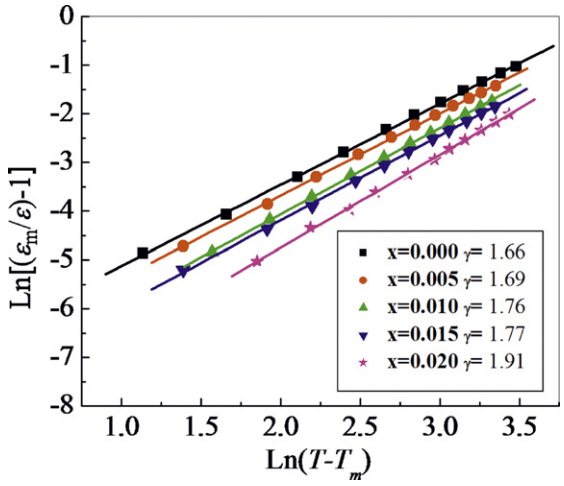

Fig. 6. $\mathrm{Ln}[(\varepsilon_m - \varepsilon)/\varepsilon]$ as a function of $\mathrm{Ln}(T - T_m)$ for the $(1 - x/2)$ SBN53–xLS ceramics (x = 0.000, 0.005, 0.010, 0.015 and 0.020).

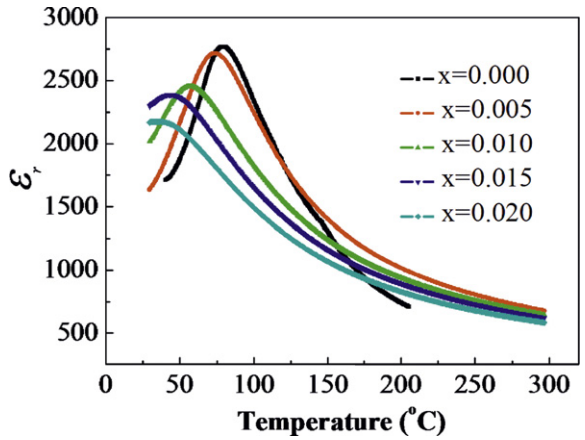

Fig. 7. Temperature dependence of ε_r for $(1 - x/2)$ SBN53–xLS ceramics measured at 1 kHz as a function of x.

maximum dielectric constant (ε_m) and the phase transition temperature (Curie temperature T_c) are dependent on x. Fig. 8 shows the transition temperature T_c and the maximum dielectric constant ε_m of the samples as a function of x. From Fig. 8, it is found that the maximum dielectric constant ε_m decreases gradually from 2772 to 2185 with increasing x. T_c shows similar variational trend with ε_m, and obtains the minimum value of 33 °C at x = 0.20. The decreasing of T_c may be due to the distortion of crystal lattice caused by Li^+ introduction in C sites and Sb^{5+} substitution for Nb^{5+} in B sites.

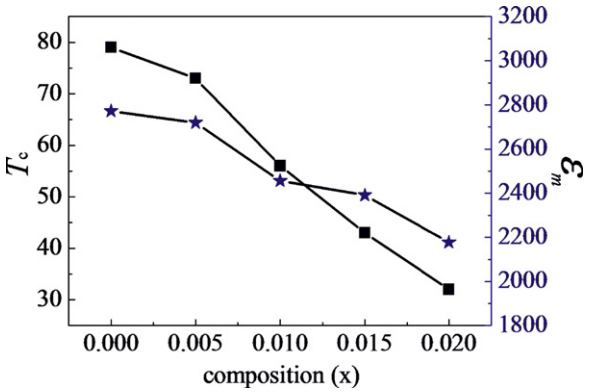

Fig. 8. ε_m and T_c of the $(1 - x/2)$ SBN53–xLS ceramics measured at 1 kHz as a function of x.

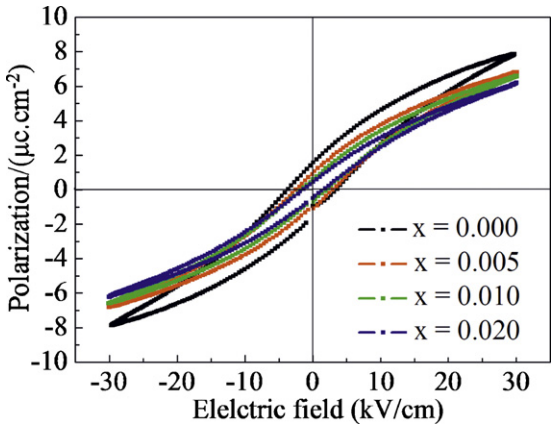

Fig. 9. P–E hysteresis loops of $(1 - x/2)$ SBN53–xLS ceramics measured at room temperature as a function of x.

The polarization levels versus applied electrical field (P–E) hysteresis loops of all the compositions measured at room temperature is shown in Fig. 9. It can be seen from Fig. 9 that the P–E hysteresis loops become much slimmer when increasing the $LiSbO_3$ content. The remnant polarization (P_r) and coercive field (E_c) of the ceramics decrease gradually with increasing x from 0.000 to 0.020. As mentioned in Fig. 8, decreasing of T_c to near room temperature improves the structure symmetry of unit cell, making the ferroelectric properties deteriorate and even disappear when doping higher amount of $LiSbO_3$.

4. Conclusions

Tungsten bronze structure $Sr_{0.53}Ba_{0.47}Nb_2O_6$ ceramics doping with $LiSbO_3$ were prepared by conventional mixed-oxide method. The phase structure, microstructure, dielectric properties and ferroelectric properties of obtained ceramics as a function of $LiSbO_3$ content were investigated. The results showed that pure tungsten bronze structure could be obtained in all ceramics and $LiSbO_3$ additive could promote densification and reduce the sintering temperature. The dielectric characteristics showed diffuse phase transition phenomena for all samples, which was proved by linear fitting of the modified Curie–Weiss law. The electrical properties of $(1 - x/2)$ $Sr_{0.53}Ba_{0.47}Nb_2O_6$–$x$$LiSbO_3$ ceramics greatly depended on x. With increasing $LiSbO_3$ content, the maximum dielectric constant ε_m decreased from 2772 to 2185, and the transition temperature T_c decreased gradually to near room temperature. Normal ferroelectric hysteresis loops could be observed in all compositions, but the remnant polarization (P_r) and coercive field (E_c) all decreased gradually with increasing $LiSbO_3$ content.

Acknowledgements

This work was supported by Foundation of Doctorial Program in China (Grant No. 20070718004), National Science Foundation of China (NSFC) (Grant No. 20771070) and the Fundamental Research Funds for the Central Universities (Program No. 2010ZYGX011).

References

[1] P.V. Lenzo, E.G. Spencer, A.A. Ballman, Appl. Phys. Lett. 11 (1967) 23–24.
[2] S.B. Qadri, J.A. Bellotti, A. Garzarella, T. Wieting, D.H. Wu, Appl. Phys. Lett. 89 (2006) 222911.
[3] J. de Los, S. Guerra, R.G. Mendes, J.A. Eiras, J. Appl. Phys. 103 (2008) 014102.
[4] S. Lee, R.H.T. Wilke, S. Trolier-McKinstry, S.J. Zhang, C.A. Randall, Appl. Phys. Lett. 96 (2010) 031910.
[5] M.D. Ewbank, R.R. Neugaonkar, W.K. Cory, J. Feinberg, J. Appl. Phys. 62 (1987) 374–380.
[6] E. Martín Rodríguez, D. Jaque, J. García Sole, R. Pankrath, Appl. Phys. Lett. 92 (2008) 181107.

[7] P. Haro-Gonzalez, I.R. Martin, L.L. Martin, S.F. Leon-Luis, C. Perez-Rodriguez, V. Lavin, Opt. Mater. 33 (2011) 742–745.
[8] M. Cuniot-Ponsard, J.M. Desvignes, A. Bellemain, F. Bridou, J. Appl. Phys. 109 (2011) 014107.
[9] S. Nishiwaki, M. Kishi, J. Appl. Phys. 35 (1996) 5137.
[10] T. Imai, S. Yagi, K. Yamazaki, M. Ono, Jpn. J. Appl. Phys. 38 (1999) 1984–1988.
[11] Y.B. Yao, W.C. Liu, C.L. Mak, K.H. Wong, H.L. Tam, K.W. Cheah, Thin Solid Films 519 (2010) 52–57.
[12] X. Hao, Y.F. Yang, J. Mater. Sci. 42 (2007) 3276–3279.
[13] S.R. Jigajeni, S.V. Kulkarnia, Y.D. Kolekarb, S.B. Kulkarnic, P.B. Joshi, J. Alloys Compd. 492 (2010) 402–405.
[14] Z.P. Yang, R. Gu, L.L. Wei, H.M. Ren, J. Alloys Compd. 504 (2010) 211–216.
[15] H.Y. Lee, R. Freer, J. Mater. Sci. 33 (1998) 1703–1708.
[16] T. Kimura, S. Miyamoto, T. Yamaguchi, J. Am. Ceram. Soc. 73 (1990) 127–130.
[17] L.L. Wei, Z.P. Yang, Y.F. Chang, R. Gui, J. Am. Ceram. Soc. 91 (2008) 1077–1082.
[18] M.H. Francombe, Acta Crystallogr. 13 (1960) 131–140.
[19] L.L. Wei, Z.P. Yang, R. Gui, H.M. Ren, J. Am. Ceram. Soc. 93 (2010) 1978–1983.
[20] Y.F. Chang, Z.P. Yang, L.R. Xiong, Z.H. Liu, Z.L. Wang, J. Am. Ceram. Soc. 91 (2008) 2211–2216.
[21] X.L. Chao, Z.P. Yang, M.Y. Dong, J. Alloys Compd. 477 (2009) 243–249.
[22] N. Jiang, B.J. Fang, J. Wu, Q.B. Du, J. Alloys Compd. 509 (2011) 2420–2424.
[23] C. Duran, G.L. Messing, S. Trolier-McKinstry, J. Mater. Sci. 37 (2002) 5041–5049.